ACS APPLIED MATERIALS & INTERFACES

Research Article

www.acsami.org

Graphene Quantum Dots from a Facile Sono-Fenton Reaction and Its Hybrid with a Polythiophene Graft Copolymer toward Photovoltaic Application

Parimal Routh, Sandip Das, Arnab Shit, Partha Bairi, Pradip Das,[‡] and Arun K. Nandi*

Polymer Science Unit, Indian Association for the Cultivation of Science, Jadavpur, Kolkata 700 032, India

Supporting Information

ABSTRACT: A new and facile approach for synthesizing graphene quantum dots (GQDs) using sono-Fenton reaction in an aqueous dispersion of graphene oxide (GO) is reported. The transmission electron microscopy (TEM) micrographs of GQDs indicate its average diameter as ~5.6 ± 1.4 nm having a lattice parameter of 0.24 nm. GQDs are used to fabricate composites (PG) with a water-soluble polymer, polythiophene-*g*-poly[(diethylene glycol methyl ether methacrylate)-*co*-poly(*N*,*N*-dimethylaminoethyl methacrylate)] [PT-*g*-P(MeO$_2$MA-*co*-DMAEMA), P]. TEM micrographs indicate that both P and PG possess distinct core−shell morphology and the average particle size of P (0.16 ± 0.08 μm) increases in PG (0.95 ± 0.45 μm). Fourier transform infrared and X-ray photoelectron spectrometry spectra suggest an interaction between −OH and −COOH groups of GQDs and −NMe$_2$ groups of P. A decrease of the intensity ratio of Raman D and G bands (I_D/I_G) is noticed during GQD and PG formation. In contrast to GO, GQDs do not exhibit any absorption peak for its smaller-sized sp^2 domain, and in PG, the $\pi-\pi^*$ absorption of polythiophene (430 nm) of P disappears. The photoluminescence (PL) peak of GQD shifts from 450 to 580 nm upon a change in excitation from 270 to 540 nm. PL emission of PG at 537 nm is quenched, and it shifts toward lower wavelength (~430 nm) with increasing aging time for energy transfer from P to GQDs followed by *up-converted* emission of GQDs. Both P and PG exhibit semiconducting behavior, and PG produces an almost reproducible photocurrent. Dye-sensitized solar cells (DSSCs) fabricated with an indium−titanium oxide/PG/graphite device using the N719 dye exhibit a short-circuit current (J_{sc}) of 4.36 mA/cm^2, an open-circuit voltage (V_{oc}) of 0.78 V, a fill factor of 0.52, and a power conversion efficiency (PCE, η) of 1.76%. Extending the use of GQDs to fabricate DSSCs with polypyrrole, both V_{oc} and J_{sc} increase with increasing GQD concentration, showing a maximum PCE of 2.09%. The PG composite exhibits better cell viability than the components.

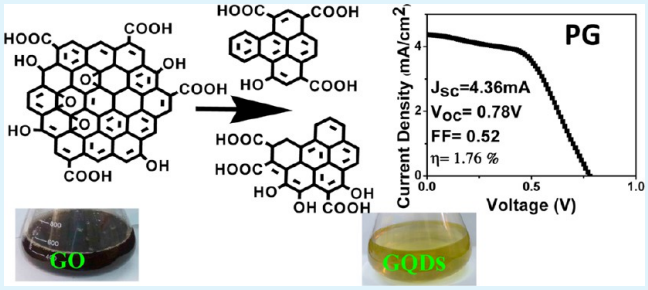

KEYWORDS: *graphene quantum dot, sono-Fenton reaction, polythiophene graft copolymer, up-converted emission, photoconductivity*

INTRODUCTION

To utilize graphene in microelectronic devices and to successfully tailor the band gap of graphene, a promising approach is to transform the 2D graphene sheets into 0D graphene quantum dots (GQDs). The distinct electronic properties of GQDs arising from the quantum confinement and edge effects promise its applications in new generation materials, such as bioimaging,[1−4] photovoltaics,[5−8] and light-emitting diodes.[9,10] The highly important synthesis of GQDs is still at the initial stage, and some approaches are established to synthesize GQDs, including an electrochemical method,[11] cutting of large GO sheets via a hydrothermal route,[12] preoxidization,[13] conversion of C_{60} molecules,[14] conventional organic synthesis,[15] exfoliation of pristine graphite using ionic liquid,[16] electron-beam lithography,[17] etc. However, the above methods suffer from some major disadvantages, e.g., the use of harsh conditions (i.e., high temperature, organic solvent, ionic liquid, etc.), time consuming, low yield, poor optoelectronic properties, and reduced solubility in an aqueous medium. This causes difficulty for practical applications, demanding a new facile synthetic route for the preparation of high-quality GQDs on a large scale. Zhou et al.[18] have reported a new strategy to prepare GQDs by photo-Fenton reaction, and here we report an improved synthetic technique for the formation of GQDs by using sono-Fenton reaction. Sono-Fenton reaction is the Fenton reaction under sonicated conditions; on the other hand, photo-Fenton reaction is the Fenton reaction under light. Thus, the sono-Fenton reaction is more facile to execute than the photo-Fenton reaction because it is more favorable for the large-scale synthesis of GQDs with small size with interesting PL properties.

Nowadays, polythiophene (PT) is the most widely investigated class of conjugated material because of its high environmental stability in various redox states and excellent

Received: September 16, 2013
Accepted: November 18, 2013
Published: November 18, 2013

optoelectronic and charge-transport properties. This makes PT an outstanding material for application in electronic devices, such as light-emitting diodes,[19] photovoltaic devices,[20,21] logic gates,[22] and field-effect transistors.[23] In spite of the excellent properties of PT, processability is a vital problem because of its low solubility in an aqueous medium. Introducing hydrophilic side chains by grafting upon a PT backbone makes the polymer water-soluble[24] and also processable, extending its use in different biotechnological applications. Furthermore, side chains can tune the sensing and optoelectronic properties of the native polymer.[25] It has been reported that side-chain branching in PT can enhance the communication between the neighboring chains and diminish the charge recombination possibility.[26] Side chains may also enlarge the conjugation length and broaden the absorption spectrum of the polymer by importing defects, and it may improve the material properties, which could be helpful for solar cell application.[27−30]

At present, the GQD-based solar cell is highly important because GQDs are large-band-gap semiconductors with distinctive physical properties of high chemical stability, large surface area, and huge exciton binding energies. This makes it an important material because of its prospective applications in optoelectronic devices, and Li et al.[11] have reported that the green-luminescent GQDs act as potential electron acceptors for application in photovoltaics. Gupta et al.[31] have demonstrated that composites of GQDs with poly(3-hexylthiophene-2,5-diyl) and poly[2-methoxy-5-(2-ethylhexyloxy)-1,4-phenylenevinylene] improve the solar cell efficiency significantly. Here we report a facile sono-Fenton synthesis of GQDs and formation of a composite material (PG) by simple mixing of GQDs with a water-soluble dual-responsive (pH and temperature) PT graft copolymer, polythiophene-*g*-poly[(diethylene glycol methyl ether methacrylate)-*co*-poly(*N*,*N*-dimethylaminoethyl methacrylate)] (P).[32] The carboxyl groups (−COOH) of GQDs attach to the dimethylamino groups of the polymer (P) chain. Thus, GQDs quench the fluorescence of P by an energy-transfer process, and then a *delayed up-converted emission* of GQDs begins to show a gradual increase of the PL intensity of GQDs with increasing aging time. The PG composite exhibits good photoconductivity and has better cell viability than that of components, providing a scope to fabricate photovoltaic and biotechnological devices. In order to extend the application of GQDs to other conducting polymers particularly for photovoltaic application, we have also studied GQD−polypyrrole (PPy) composites (PPG) at different compositions. The power conversion efficiency (PCE) of the PPG composites also increases with an increase in the GQD concentration.

EXPERIMENTAL SECTION

Materials. The monomers (3-thiophenylethanol), diethylene glycol methyl ether methacrylate (MeO_2MA), *N*,*N*-dimethylaminoethyl methacrylate (DMAEMA), and graphite powder were purchased from Aldrich Chemicals. Sodium nitrate ($NaNO_3$) was obtained from Loba Chemicals (Mumbai, India), and potassium permanganate was purchased from Mark Chemicals (Mumbai, India). The monomers MeO_2MA and DMAEMA were purified by passing through a neutral alumina and a basic alumina column, respectively. The ligand 1,1,4,7,10,10-hexamethyltriethylenetetramine (HMTETA; Aldrich) was used as received. The catalyst CuCl (Loba Chemicals) was purified by washing with 10% HCl in water followed by methanol and diethyl ether in a Schlenk tube under a nitrogen atmosphere. The solvents dichloromethane, anisole, and chloroform (Loba Chemicals) were purified by distillation, and water was purified by double distillation before use.

Synthesis of GQDs Using Sono-Fenton Reaction. A new and facile sono-Fenton technique was used for the preparation of GQDs (Scheme 1). In a typical experiment, 50 mg of graphene oxide (GO) was synthesized using Hummer's method, and it was completely dissolved in 100 mL of deionized water. Then 20 mL of 30% H_2O_2 was added under magnetic stirring, and $FeCl_3$ (10 mg in 5 mL of water) was mixed into the above solution under vigorous stirring at pH 7. The reaction was initiated by keeping the reaction mixture in an ultrasonication bath (80 W), and it was sonicated for 4 h. The reaction products were then dialyzed in ultrapure water for 2 days to remove the iron ions. Complete removal of the iron ions was confirmed from the separate addition of NH_4OH to the washed part by the absence of a reddish-brown color of the iron hydroxide precipitate.

Scheme 1. Synthetic Procedure of GQDs

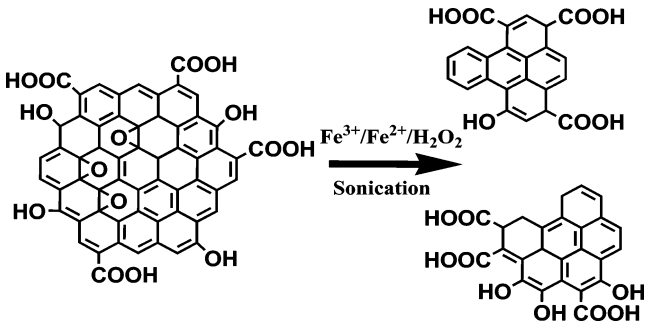

Synthesis of Polythiophene-*g*-poly[(diethylene glycol methyl ether methacrylate)-*co*-poly(*N*,*N*-dimethylaminoethyl methacrylate)] (P). The polymer was synthesized by atom-transfer radical polymerization (ATRP) using CuCl as the catalyst and HMTETA as the ligand, following a procedure consisting of three steps presented in ref 32: (i) preparation of 3-[1-ethyl-2-(2-bromoisobutyrate)]-thiophene (thiophene initiator, TI), (ii) preparation of 2,5-poly[3-[1-ethyl-2-(2-bromoisobutyrate)]]thiophene (polythiophene macroinitiator, PTI), and (iii) ATRP polymerization to produce polythiophene-*g*-poly[(diethylene glycol methyl ether methacrylate)-*co*-poly(*N*,*N*-dimethylaminoethyl methacrylate)] [PT-*g*-P(MeO_2MA-*co*-DMAEMA), P]. The polymer produced was collected, redissolved in tetrahydrofuran (THF), and precipitated into excess petroleum ether. This process was repeated for three times to eliminate the excess amount of monomer entrapped within the polymer. The THF solution of the sample was then passed through a silica column followed by solvent evaporation to obtain copper-free P.[32]

Preparation of a Composite Material of P and GQDs (PG). A total of 2 mL of a 0.2% (w/v) aqueous P solution was taken in a sealed glass tube followed by the addition of 6.8 mL of a 0.017% (w/v) GQD solution (w/v), and the resulting solution was mixed well by sonication. The homogeneous solution was then freeze dried to obtain the solid composite PG, where the weight fraction of GQDs was 0.22.

Preparation of PPy and Its Composite with GQDs (PPG). A total of 182 μL of pyrrole was dispersed in a 5 mL 0.2 M acetic acid solution, and then 5 mL of a ammonium persulfate solution was added at a 1:1 molar ratio of APS and pyrrole. The mixture was kept at 30 °C for 24 h to complete the polymerization. The mixture was then filtered and washed repeatedly with distilled water and methanol. Finally, it was dried at first in air and finally in a vacuum at 30 °C for 3 days.

A total of 2 mL of a 0.2% (w/v) aqueous dispersion of PPy was taken in three glass tubes, and 6.8 mL portions of 0.01, 0.02, and 0.03% (w/v) GQD solutions were added to each tube to prepare PPG1, PPG2, and PPG3 composites, respectively. They were mixed and homogenized well by sonication to get a good dispersion.

Morphology. The shape, size, and dispersity of the GQDs were monitored by a transmission electron microscope (JEOL 2010EX) operated at a 200 kV voltage and fitted with a CCD camera. A specimen for the transmission electron microscopy (TEM) study was made by spreading a small drop of the sample solution on a carbon-

coated copper grid followed by drying completely in air at 25 °C and finally in a vacuum at 30 °C for about 3 days. The surface morphologies of the dried films of GQDs were studied using an atomic force microscope (Veeco, model AP 0100). The atomic force microscopy (AFM) study was conducted in noncontact mode at a resonance frequency of the tip end of ∼250 kHz. A GQD solution was cast on a fresh mica surface and dried at 30 °C for 3 days in air.

Spectroscopy. The UV−vis spectra of different samples were studied in aqueous solutions using a 1 cm quartz cell in an UV−vis spectrophotometer (model 8453, Hewlett-Packard). The Fourier transform infrared (FTIR) spectra of the hybrids were taken from KBr pellets of the samples in a Shimadzu FTIR instrument (model 8400S). The PL spectra were recorded from aqueous solutions/dispersions of the pure and composite samples in a 1 cm quartz cell in a FluoroMax-3 (Horiba-Jobin Yvon) instrument. Raman spectra were performed using a Raman triple spectrometer (model T-64000, Horiba-Jobin Yvon) fitted with a synapse detector. The sample was excited with a 514.5 nm laser (Spectra Physics, model Stabilite 2017). X-ray photoelectron spectrometry (XPS) spectra were recorded with the help of a focused monochromatized A1 Kα X-ray source (1486.8 eV) in an Omicron Nano Technology (model 0571) XPS spectrometer.

Conductivity Measurement. The direct-current (dc) conductivity at 30 °C of the freeze-dried samples was measured using the two-probe method by sandwiching the sample between two indium−titanium oxide (ITO) conducting strips of 1 mm width. All of the measurements were carried out in a vacuum. The area of the sample was 0.01 cm^2, and the thickness of the sample was measured by a screw gauge. The conductivity of the sandwiched sample was measured by an electrometer (Keithley, model 617) at 25 °C using the equation

$$\sigma = \frac{1}{R}\frac{l}{a}$$

where l is the thickness, a is the area, and R is the resistance. The $I-V$ characteristic curves of the samples were studied at 25 °C using the same sample by applying voltage from −5 to +5 V, and the current was measured at each applied voltage.

Dye-Sensitized Solar Cell (DSSC) Construction. The PG and PPG substrates were sensitized by immersing them into an 0.5 mM ethanolic solution of the N719 dye (a ruthenium complex dye) for approximately 20 min. The counter electrode was a graphite-coated ITO glass plate (2 × 2 cm^2). The iodide/triiodide-based electrolyte solution, consisting of 0.5 M KI and 0.05 M I_2 in γ-butyrolactone, was placed on the active electrode area dropwise. The average active electrode area was around 0.78 cm^2. The electrodes were separated by a 60-μm Parafilm and sandwiched together with clips. A small space of bare ITO glass was uncovered for a wire connection on the anode. The configuration of the solar cell was achieved by putting the PG/PPG face of the ITO substrate on top of the counter electrode in a face-to-face fashion. The dc between the two electrodes was measured using a Keithley source meter (model 2401). The currents were measured by illumination with white light from a 150 W xenon lamp source (Newport Corp., Springfield, OH; model 67005). The illumination was 100 mW/cm^2 for all acquired data.

Cytotoxicity Test: MTT Assay. 3-(4,5-Dimethylthiazol-2-yl)-2,5-diphenyltetrazolium bromide (MTT) assay was used to measure the cell viability. HeLa cells were seeded in a 24-well plate in the presence of 500 μL of Dulbecco's modified Eagle medium (DMEM) media containing 10% fetal bovine serum and 1% penicillin/streptomycin and allowed to grow overnight. The cells were then incubated with the GQDs, P, and PG for 24 h. The final concentrations were 3.92, 18.18, 33.33, 57.14, 75, and 100 μg/mL, respectively. The cells were washed with a phosphate-buffered saline solution. Then, a fresh 500 μL of DMEM media was added to each well followed by the addition of 50 μL of MTT (5 mg/mL in water). After an incubation period of 4 h, supernatant liquid was removed from each well. The violet formazan was dissolved in 500 μL of a sodium dodecyl sulfate solution in a *N*,*N*-dimethylformamide/water mixture. The absorbance of the solution was measured at 570 nm using a BioTek SynergyMx microplate reader. The relative cell viability was measured by assuming 100% cell viability with no sample.

RESULTS AND DISCUSSION

In Figure 1, the TEM micrographs of GO and GQDs are presented for comparison purposes. Figure 1a presents the

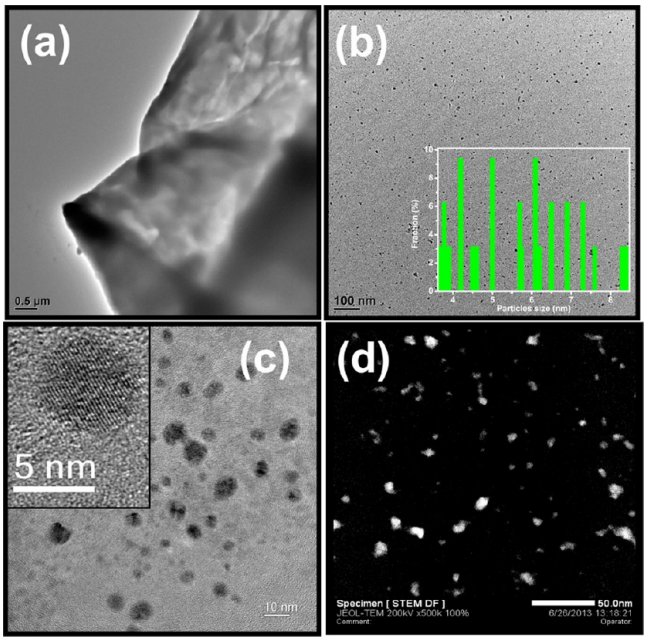

Figure 1. TEM micrographs of (a) GO, (b) GQDs (inset: size distribution), and (c) GQDs at 10 times higher magnification of part b (inset: HRTEM image of GQDs) and (d) dark-field image of GQDs.

wrinkled GO sheet of very large (micrometer) dimension, and upon sono-Fenton reaction (Scheme 1), this large GO sheet disintegrates into tiny GO particles (Figure 1b), which may be called GQDs. The diameters of the GQDs are mainly distributed in the range of 3−10 nm with an average diameter of 5.6 ± 1.4 nm (Figure 1b,c and the inset of Figure 1b). A representative high-resolution TEM (HRTEM) image of an individual GQD is presented in the inset of Figure 1c, and the fringe pattern indicates a crystalline lattice parameter of 0.24 nm of GQDs. Figure 1d exhibits the dark-field image of GQDs, and from this figure, it is apparent that GQDs are nearly monodispersed nanoparticles. So, from the TEM micrographs, it is very much evident that during the sono-Fenton reaction the macrosized GO is easily disintegrated into tiny-sized GQDs. In Figure 2a−c, an AFM height image of GQDs is presented, and good dispersion of GQDs is clearly noticed in the micrograph. Its height profile ranges from 0.2 to 5 nm, suggesting that during the sono-Fenton reaction a monolayer to a few layers of GQDs are formed. In Figure 2c, the histogram of the height image indicates a most probable distribution at ∼0.5−0.7 nm, suggesting formation of the majority of the graphene monolayer sheets during the sono-Fenton reaction.[33]

TEM micrographs of P and PG samples cast from their aqueous solutions are presented in Figure 3a,b. The average particle size of P increases dramatically in PG (0.95 ± 0.45 μm) compared to that of pure P (0.16 ± 0.08 μm). Another interesting feature is that both P and PG (Figure 3a,b) exhibit distinct core−shell morphology. In an aqueous solution, the P samples remain in the solution state by forming miceller arrangements with the insoluble PT core and soluble grafted

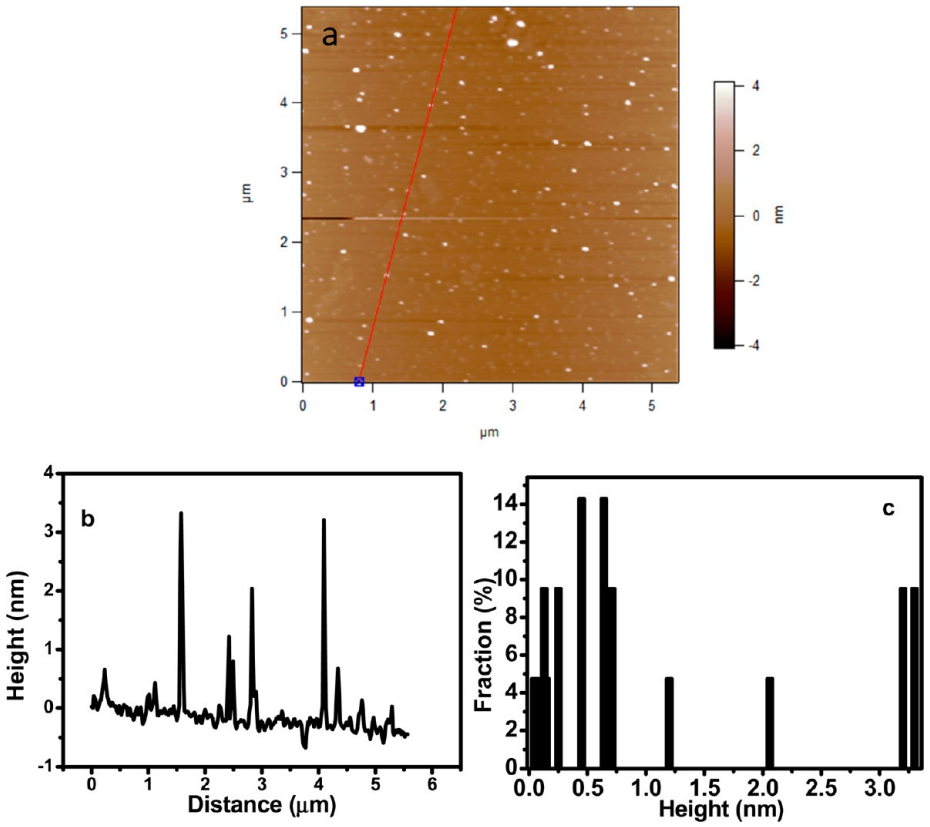

Figure 2. (a) AFM image of the GQDs, (b) corresponding height profile, and (c) corresponding histogram of GQDs (obtained from 30 objects).

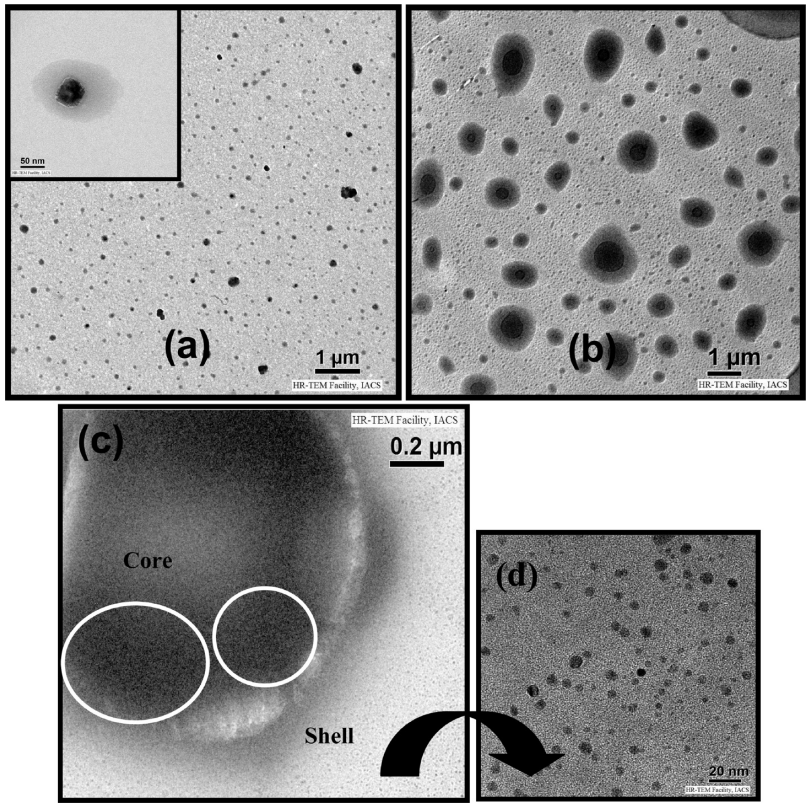

Figure 3. TEM images of (a) P (inset: enlarged image of P) and (b) PG, (c) enlarged TEM micrograph of a single core (the circles indicate the core positions with a higher density of GQDs), and (d) enlarged TEM image of the shell structure of PG of part c.

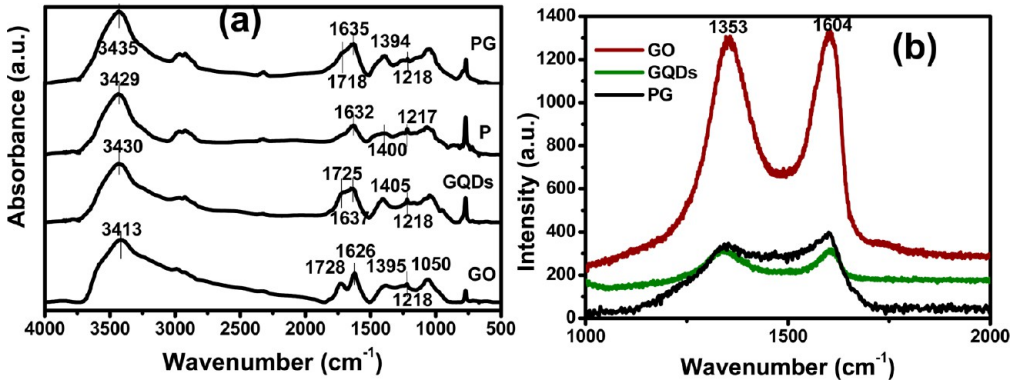

Figure 4. (a) FTIR spectra of GO, GQDs, P, and PG and (b) Raman spectra of GO, GQDs, and PG.

chains at the periphery. In the presence of GQDs, the $-NMe_2$ groups of PDMAEMA segments of grafted P(MeO_2MA-*co*-DMAEMA) chains become appreciably protonated by the carboxylic acid groups of GQDs, producing a quaternary ammonium ion. As a result, the coulombic repulsion between the cationic centers of the grafted chains exists, forcing the grafted chains to become uncoiled and thus spread out, which allows the solvent molecules to easily enter the graft segments, resulting in a swelled structure of micelles. The average diameter of the PT core in P is 0.08 μm, and the average shell thickness is 0.04 μm. On the other hand, the average diameter of the core in PG is 0.42 μm and the average shell thickness is 0.26 μm. Thus, a 5 times increase in the core diameter and a 6 times increase in the shell thickness occur in the PG sample. Figure 3c shows an enlarged picture of a single PG micelle, and from this figure, it is apparent that the GQDs are present both at the core and at the shell, with a larger proportion at the periphery of the core. This may be attributed to the strong electrostatic interaction between the protonated part of P and the anionic part of GQDs. Also, the $\pi-\pi$ interaction between the thiophene units of P and the sp^2 π clouds of GQDs is another attractive force for the accumulation of GQDs within the P core. At the interface, there exist both thiophene rings and $-NMe_2$ groups, causing an enhanced density of GQDs at this region. As a result, there occurs an overall increase of the miceller size of PG by 8 times compared to that of P.

The FTIR spectra in Figure 4a exhibit different types of oxygen functionalities in GO, GQDs, P, and PG. All of the samples exhibit one characteristic peak at about 3413 cm^{-1}, which is ascribed to the adsorbed water or the hydroxyl groups linked to the samples. GO has several strong characteristic peaks at 1728 cm^{-1} (>C═O carboxyl or carbonyl stretching vibration), 1626 cm^{-1} (C═C skeletal vibrations from unoxidized graphitic domains), 1395 cm^{-1} (O−H deformations in the C−OH groups), 1218 cm^{-1} (C−OH stretching vibration), and 1050 cm^{-1} (C−O stretching vibrations in epoxide). FTIR spectra of GQDs exhibit broadened peaks that can be deconvoluted as peaks at 1725 and 1637 cm^{-1} due to the >C═O and C═C bond vibrations; another sharp peak is observed at 1405 cm^{-1} for the C−OH stretching vibration, and its relative intensity is higher compared to that of GO because of more −OH bonding present in GQDs. Also, its shift to a higher energy vibration at 1405 cm^{-1} is due to hydrogen bonding with the −COOH group and other −OH groups of GQDs. P has a peak at 1400 cm^{-1} for the C−N bonding vibration,[34] but in the PG composite, this peak shifts from 1400 to 1394 cm^{-1} because of protonation from the carboxylic acid group of GQDs. The sharp peak observed at 1626 cm^{-1} of GO is shifted to 1637 cm^{-1}, and this shift to higher energy is attributed to the decreasing size of the graphitic clusters in GQDs. In PG, it remains at the intermediate position with that of P and that of GQDs. It is also important to note that the 3413 cm^{-1} peak of GO has shifted to 3430 cm^{-1} in GQDs, and the shift to higher energy is due to intermolecular hydrogen bonding with other −OH and −COOH groups of GQDs. In PG, this 3430 cm^{-1} peak shifts to 3435 cm^{-1} for interaction between the −OH groups of GQDs and the dimethylamino groups of polymer P.

The Raman spectra (Figure 4b) of GO, GQDs, and PG reveal the existence of the D (1353 cm^{-1}) and G (1604 cm^{-1}) bands corresponding to the disorder-induced phonon mode and Raman-allowed phonon mode of vibrations, respectively.[18] Figure 4b shows that for GQDs the I_D/I_G value (0.90) is lower compared to that of GO (0.96). This result indicates that during sono-Fenton cleavage of GO the GQDs are reduced by Fenton's reagent. In PG, the I_D/I_G value (0.86) is also lower than that of GQDs because during the addition of P the GQDs become further reduced because of the presence of the reducing $-NMe_2$ group in P.

XPS measurement is used to study elemental analysis as well as the chemical-bonding environment of GQDs, P, and PG. Figure 5 represents the XPS spectra of GQDs, P, and PG; from the spectra, O 1s and C 1s peaks are observed at 531.9 and

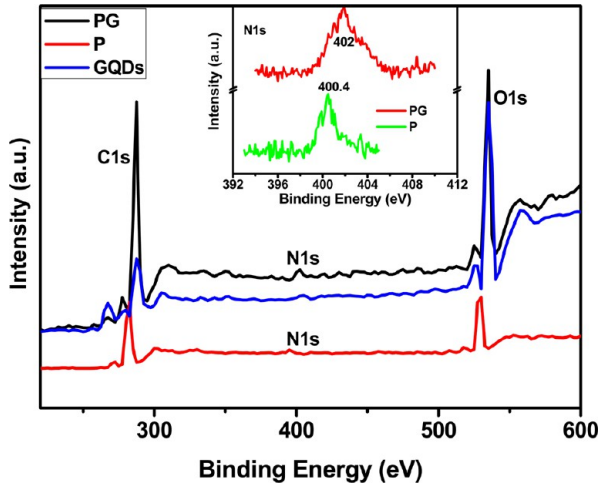

Figure 5. XPS spectra of P, GQDs, and PG (inset: enlarged spectra for the nitrogen atom).

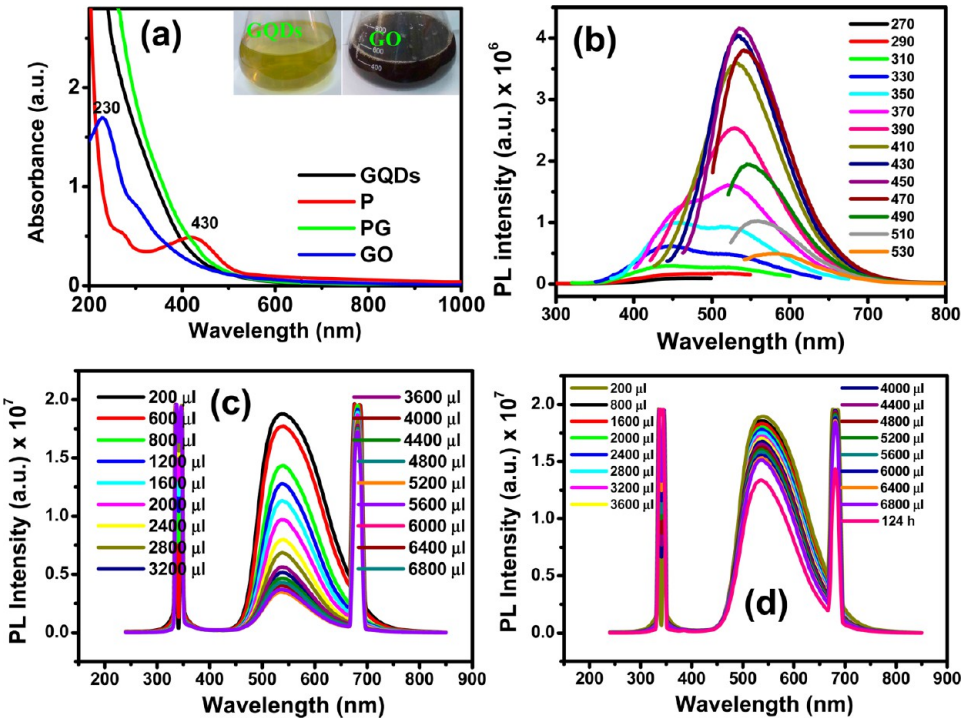

Figure 6. (a) UV−vis absorption spectra of GO, GQDs, P, and PG (inset: photograph of the GO and GQDs taken under normal light). (b) Excitation-dependent PL spectra of the GQDs. (c) PL spectra of PG at different GQD volumes for excitation at 340 nm. (d) PL spectra of P with the addition of different amounts of water for excitation at 340 nm (blank experiment).

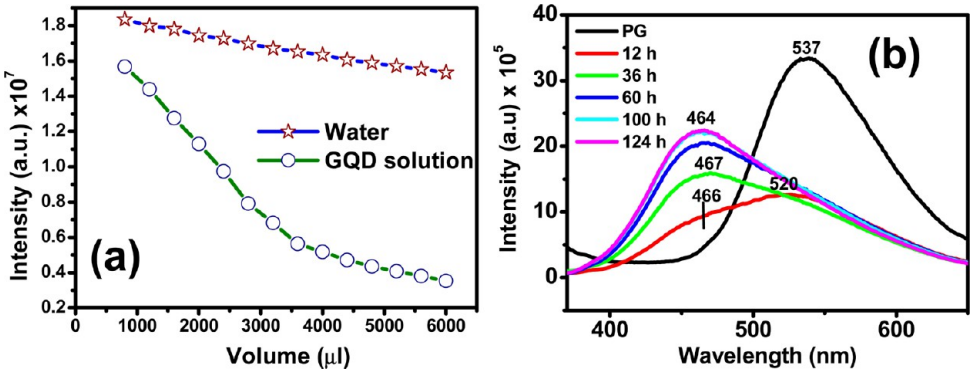

Figure 7. (a) PL intensity versus volume of diluents for P with the addition of a water and GQD solution. (b) Intensity versus wavelength of PG composites at different aging times for excitation at 340 nm.

284.5 eV, respectively, for all of the samples. On the other hand, the N 1s peak is present only in P and PG because the polymer contains nitrogen elements. Because of the very low atom percentage of sulfur in P and PG, the characteristic peak for sulfur is not distinctly observed. It is important to note that the N 1s peak at 400.4 eV has shifted to higher binding energy at 402 eV (Inset of Figure 5), indicating the presence of strong interaction between P and GQDs. Possibly protonation of the dimethylammonium group of P by the carboxylic acid groups of GQDs, followed by ionic interaction between the resulting cationic and anionic species, is the cause of strong interaction between P and GQDs.

The optical properties of GQDs, P, GO, and PG are assessed by the UV−vis absorption and photoluminescence (PL) spectra (Figure 6). In the inset of Figure 6a, the photographs produced under ordinary light indicate that aqueous dispersion of GO has a black color, but GQDs exhibit a light-yellowish-green color, differentiating the two graphenes that differ greatly in size. The UV−vis absorption spectrum of P (Figure 6a) shows a typical absorption peak at λ_{max} = 430 nm, ascribed to the $\pi-\pi^*$ transition of the conjugated chain of P. GO exhibits a small absorption peak at 230 nm characterizing the $\pi-\pi^*$ transition of aromatic sp^2 domains of GO. However, from the UV−vis spectra of GQDs, it is clearly noticed that GQDs do not exhibit any prominent absorption peak. In the UV−vis spectra, GO has a 230 nm peak for the sp^2 domain of the carbon skeleton, but the GQD has no such peak because its peak intensity is very low because of the very small size of the sp^2 domain of the carbon skeleton.[31,35] Upon the addition of GQDs to the P solution, the 430 nm peak of P has completely disappeared. No definite reason can be afforded here, and one probable cause is the binding of P with the GQDs, causing resonance stabilization of the π electrons of the respective orbitals of the components because of their closer proximity with each other.

GQDs exhibit excitation-dependent PL behavior,[11,36,37] and with a change in the excitation wavelength from 270 to 540 nm, the PL peak moves toward the longer wavelengths from 450 to 580 nm (Figure 6b). Radovic and Bockrath[38] have explained the origin of PL in GQDs by proposing that the zigzag edges of graphene are carbene-like, with the triplet ground state being most common and emission occurring from a carbene-like triplet ($\sigma^1\pi^1$) ground state.[36,37] P has a strong PL emission peak at 537 nm,[32] but upon the addition of GQDs to the P solution, the emission peak intensity of P gradually decreases with increasing GQD concentration (Figure 6c) because of energy transfer from P to GQDs because P acts as a donor and GQDs act as acceptors. On the other hand, in a blank experiment (Figure 6d), the PL intensity of P does not exhibit any abrupt changes like that of PG because pure P is unable to energy transfer with water, but a small decrease of the intensity occurs because of the dilution factor.

Variations of the PL intensity with the volume of the GQD solution and with water are compared in Figure 7a, where the intensity of the P versus water volume plot is at much higher position than that of the the P versus GQD volume plot, clearly indicating a significant PL quenching with the addition of GQDs. Figure 7b shows that the PL emission peak of PG shifts from 537 nm toward the lower wavelength with increasing aging time and becomes almost invariant near the GQD emission peak of ca. 430 nm for excitation with a radiation of λ = 340 nm. This result can be explained by energy transfer from P to GQDs and with the help of *up-converted emission* of GQDs.[39,40] At an aging time of ca. 12 h, the energy-transfer process between GQDs and P is almost complete, as is evident from the lowest PL intensity of PG at 537 nm, and after that, the delayed *up-converted emission* of GQDs starts and the PL intensity of GQDs gradually increases with increasing aging time. It is interesting to note that GQDs do not exhibit any emission peak in the PG solution when directly excited at 340 nm. A probable reason is that screening of GQDs by the polymer chain had an immediate effect.

Electronic and Optoelectronic Properties. The valence and conduction bands of graphene intersect at a particular point, called the Dirac point, where electrons in graphene behave as massless fermions.[41,42] So, graphene is a zero-band-gap material, and semiconducting properties are completely impossible. Changing the band gap of graphene is very important to improving its electronic properties. The conductivity of graphene is very high, but after the graphene sheet is broken to form GQDs, it exhibits a conductivity of ~3 × 10^{-7} s/cm, which matches very well with that of semiconducting materials. P shows a conductivity of ~1.0 × 10^{-9} s/cm, which value is close to that of an insulator, but the PG composite exhibits a conductivity of ~3 × 10^{-6} s/cm. The increase in the conductivity in the PG sample may be attributed to the reducing property of P, which increases the graphitic domains (cf. Raman spectra) of GQDs, producing a lower-band-gap material. Also, the GQDs can π-stack with the thiophene units of the polymer because of their closer proximity with each other for strong ionic interaction between the components, creating new paths for conduction. Possibly, a combination of the above two effects causes higher conductivity of PG than that of the components.

The $I-V$ characteristic curves of GQDs and PG are presented in parts a and b of Figure 8, respectively. Both systems exhibit almost similar patterns, indicating semiconducting behavior. We have recorded $I-V$ characteristics of

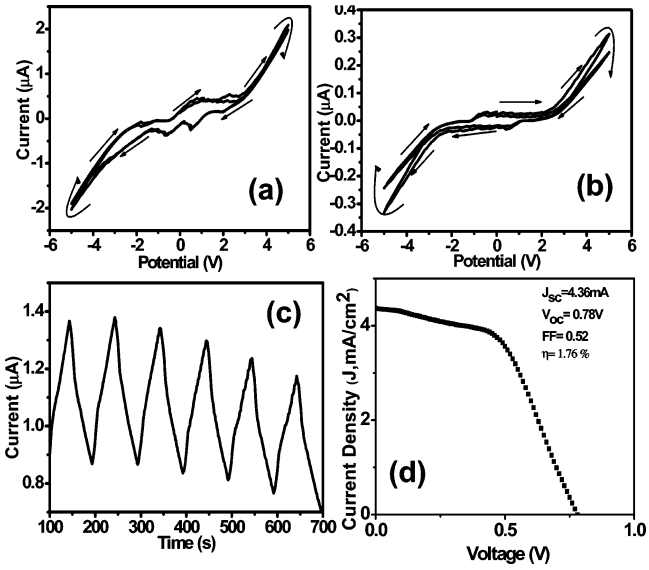

Figure 8. $I-V$ characteristic curves of (a) GQDs and (b) PG. (c) Photocurrent cycles of PG for "on" and "off" switching with white light. (d) $J-V$ curve of PG.

ITO/PG/ITO devices under alternating dark and illumination conditions at a time interval of 50 s, and Figure 8c presents the photocurrent of the PG sample. It is evident from the different "on" and "off" cycles that PG produces almost a stable photocurrent particularly at the first three or four cycles. The minor instability after three cycles may be attributed to the presence of a ~90% nonconducting part present in P,[32] where the DMAEMA part may cause easier degradation to PT.[43] Therefore, considering the fully organic material, the reversibility of the photocurrent is considerably good.[44]

We have fabricated a DSSC with an ITO/PG/graphite device using 100 mW/cm^2 illumination conditions. Under this illumination, the $J-V$ characteristic plot (Figure 8d) shows a photovoltaic behavior with a short-circuit current (J_{sc}) of 4.36 mA/cm^2, an open-circuit voltage (V_{oc}) of 0.78 V, a fill factor (FF) of 0.52, and a PCE (η) of 1.76%. After absorbing white light by the N-719 dye in the above-fabricated DSSC, an electron of the dye is promoted to its excited state. The excited electron enters into the conduction band of the PG composite, and then it flows to the external circuit. The process is facilitated by the GQDs of the composite by enhancing the electron mobility of the conducting polymer P.[45,46] This promotes effective charge separation with a negative charge in the PG composite and a positive charge on the surface of the adsorbed dye molecule. This yields the above solar cell parameters in the PG composite.

Composites of GQDs with PPy. In order to check the capability of GQDs to make composites with other conducting polymers, we have chosen PPy because of the presence of a nitrogen atom in its ring, which can interact with the carboxylic acid group of GQDs. We have studied the PL property PPG2 dispersion in water for excitation at 340 nm at 30 °C. Interestingly, the system exhibits a 2 and 3 times increase of the PL intensity of GQDs upon aging for 72 and 96 h, respectively, with a blue shift of 10 nm from that of GQDs (Supporting Information Figure S1). A possible reason may be slow complex formation of PPy with GQDs through the acid−base-type interaction between the −COOH groups of GQDs and the nitrogen atom of PPy. The slowness of complexation may

be attributed to the high viscosity of the medium hindering the conformational motion of the PPy chain for interaction with the −COOH groups of GQDs. This complex formation would be, therefore, beneficial to the solar cell fabrication, and we fabricated DSSCs with PPy and GQDs at three different compositions using the N719 dye. It is evident from the figure (Figure 9) that both V_{oc} and J_{sc} increase with increasing GQD

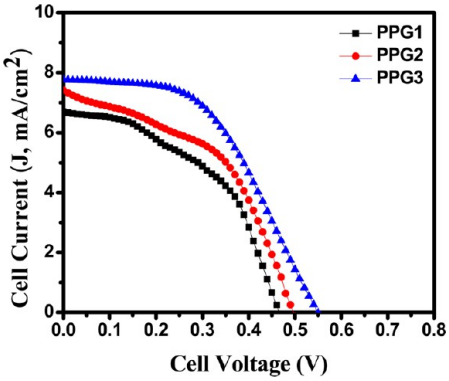

Figure 9. $J-V$ curves of PPG1, PPG2, and PPG3 composites.

Table 1. DSSC Parameters of PG and PPG Composites

sample	mol % (w/v) of GQD in the composites	J_{sc}, mA/cm^2	V_{oc}, V	FF	PCE (η, %)
PG	0.017	4.36	0.78	0.52	1.76
PPG1	0.01	6.69	0.46	0.29	0.89
PPG2	0.02	7.42	0.49	0.32	1.16
PPG3	0.03	7.8	0.54	0.50	2.09

concentration (Table 1) with a maximum PCE of 2.09% for the PPG3 sample. Thus, both the PG and PPG composites of GQDs exhibit photovoltaic properties. In a comparison of the respective solar cell parameters (Table 1), it is noted that J_{sc} is much lower and V_{oc} is much higher in the PG composite compared to those of PPG composites. The J_{sc} value of the composite is dependent on the mobility of the electron in the material.[47] In PG, about 90% nonconducting impurity is present, while it is totally absent in the PPG composites, attributed to the increased exciton mobility in the latter systems. This is the probable cause for the lower value of J_{sc} in PG compared to that of PPG composites. The V_{oc} value depends on the band gap of the donor and acceptor.[47,48] The lowest occupied molecular orbital of P is ∼3.2 eV,[49] and that of PPy is −2.5 eV.[50] So, the band gap with GQDs is expected to be lower for P than that of PPy, causing a higher V_{oc}. As the GQD concentration in the PPG composites increases, the J_{sc} value increases because of an increase in the electron mobility in the PG composite and the V_{oc} value is almost constant with an insignificantly small increase.

It is necessary here to compare the photovoltaic behavior of composites with GQDs and other polymer hybrids presented by other workers. Gupta et al.[31] reported a bulk heterojunction (BHJ) solar cell of the P3HT composite with aniline-functionalized GQDs showing a maximum PCE of 1.14%. Liu et al.[51] reported a BHJ composed of poly(3-hexylthiophene-1,3-diyl)/graphene with PCE 1.1%. Li et al.[52] demonstrated that the introduction of GQDs into a BHJ polymer solar cell based on poly(3-hexylthiophene)/(6,6)-phenyl-C61 butyric acid methyl ester (P3HT/PCBM) resulted in a significant enhancement of the PCE, showing a maximum PCE of 5.24%. Probably the use of two donor moieties is the reason for such a large PCE value in this system. Because of the lack of an experimental setup, we are unable to fabricate a BHJ in our laboratory, but our dye-sensitized system with the N719 dye shows a reasonable PCE value for both PG and PPG composites.

MTT Assay. The PG has good up-converted emission property that may change with both the temperature and pH because the polymer is both pH- and temperature-responsive.[32] Also, it has good semiconducting properties, and both properties can be exploited to develop different biotechnological applications. We did cytotoxicity analysis of each of P, GQDs, and PG separately (Figure 10). It is apparent from the

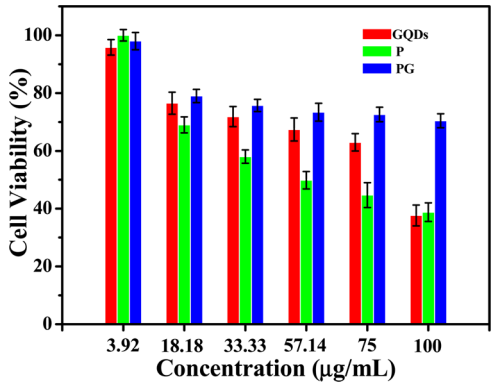

Figure 10. Cell viability at different concentrations of P, GQDs, and PG.

figure that, at a very low concentration (3.9 μg/mL) of the substrates (P, GQDs, and PG), they have very good cell viability (∼97%); however, with an increase in the concentration of the substrates, the cell viability gradually decreases. It is important to note that the cell viability of PG, however, remains constant at ∼80% even at a concentration of 100 μg/mL of PG, although at this concentration, the cell viability of each of P and GQDs is ∼40%. This suggests that the PG composite may be used as a better biomaterial than the pure polymer P or pure GQDs.

CONCLUSION

Here, we have demonstrated that the micrometer-sized GO sheets can be disintegrated into GQDs via a new and easy method using sono-Fenton reaction. The water-soluble GQDs are used to form composites with a water-soluble PT graft copolymer, with P utilizing the interaction between the −OH and −COOH groups of GQDs with the dimethylamino group of the polymer P. The synthesized P and GQDs possess bright fluorescence properties, but the PL emission peak of PG at 537 nm is quenched and shifts toward the lower wavelength (∼430 nm) with aging time because of energy transfer from P to GQDs followed by a delayed *up-converted emission* of GQDs. PG upon photoillumination produces an almost stable photocurrent, and DSSCs fabricated with an ITO/PG/graphite device using the N719 dye exhibit a PCE of 1.76%. When the use of GQDs is extended to fabricate DSSCs with other conducting polymers like PPy, it is observed that both V_{oc} and J_{sc} increase with increasing GQD concentration, showing a maximum PCE of 2.09% for the PPG3 sample. The PG

composite exhibits better cell viability than the components and can be extended for use as a better material for biotechnological applications.

■ ASSOCIATED CONTENT

Supporting Information

PL spectra of PPG2. This material is available free of charge via the Internet at http://pubs.acs.org.

■ AUTHOR INFORMATION

Corresponding Author

*E-mail: psuakn@iacs.res.in.

Present Address

‡P.D.: CAM, IACS, Jadavpur, Kolkata 700032, India.

Notes

The authors declare no competing financial interest.

■ ACKNOWLEDGMENTS

We gratefully acknowledge the CSIR [Grant 02 (0051)/12/EMR-II] for financial support. S.D. and A.S. acknowledge the DST INSPIRE program for providing a fellowship. We acknowledge Dr. N. R. Jana of CAM, IACS, for helping in MTT assay. The DST Unit of Nanoscience at IACS is gratefully acknowledged for providing access to their XPS facility.

■ REFERENCES

(1) Shen, J.; Zhu, Y.; Yang, X.; Li, C. *Chem. Commun.* **2012**, *48*, 3686−3699.

(2) Zhu, S.; Zhang, J.; Qiao, C.; Tang, S.; Li, Y.; Yuan, W.; Li, B.; Tian, L.; Liu, F.; Hu, R.; Gao, H.; Wei, H.; Zhang, H.; Sunb, H.; Yang, B. *Chem. Commun.* **2011**, *47*, 6858−6860.

(3) Chen, M.-L.; Liu, J.-W.; Hu, B.; Chen, M.-L.; Wang, J.-H. *Analyst* **2011**, *136*, 4277−4283.

(4) Li, Y.; Zhao, Y.; Cheng, H.; Hu, Y.; Shi, G.; Dai, L.; Qu, L. *J. Am. Chem. Soc.* **2012**, *134*, 15−18.

(5) Hamilton, I. P.; Li, B.; Yan, X.; Li, L.-S. *Nano Lett.* **2011**, *11*, 1524−1529.

(6) Yan, X.; Cui, X.; Li, B. S.; Li, L.-S. *Nano Lett.* **2010**, *10*, 1869−1873.

(7) Mueller, M. L.; Yan, X.; McGuire, J. A.; Li, L.-S. *Nano Lett.* **2010**, *10*, 2679−2682.

(8) Yan, X.; Cui, X.; Li, L.-S. *J. Am. Chem. Soc.* **2010**, *132*, 5944−5945.

(9) Zhang, Z.; Zhang, J.; Chen, N.; Qu, L. *Energy Environ. Sci.* **2012**, *5*, 8869−8890.

(10) Kou, L.; Li, F.; Chen, W.; Guo, T. *Org. Electron.* **2013**, *14*, 1447−1451.

(11) Li, Y.; Hu, Y.; Zhao, Y.; Shi, G. Q.; Deng, L. E.; Hou, Y. B.; Qu, L. *Adv. Mater.* **2011**, *23*, 776−780.

(12) Shen, J.; Zhu, Y.; Yang, X.; Zong, J.; Zhang, J.; Li, C. *New J. Chem.* **2012**, *36*, 97−101.

(13) Shen, J. H.; Zhu, Y. H.; Chen, C.; Yang, X. L.; Li, C. Z. *Chem. Commun.* **2011**, *47*, 2580−2582.

(14) Lu, J.; Yeo, P. S. E.; Gan, C. K.; Wu, P.; Loh, K. P. *Nat. Nanotechnol.* **2011**, *6*, 247−252.

(15) Liu, R.; Wu, D.; Feng, X.; Mullen, K. *J. Am. Chem. Soc.* **2011**, *133*, 15221−15223.

(16) Shang, N. G.; Papakonstantinou, P.; Sharma, S.; Lubarsky, G.; Li, M.; McNeill, D. W.; Quinn, A. J.; Zhoue, W.; Blackley, R. *Chem. Commun.* **2012**, *48*, 1877−1879.

(17) Ponomarenko, L. A.; Schedin, F.; Katsnelson, M. I.; Yang, R.; Hill, E. W.; Novoselov, K. S.; Geim, A. K. *Science* **2008**, *320*, 356−358.

(18) Zhou, X.; Zhang, Y.; Wang, C.; Wu, X.; Yang, Y.; Zheng, B.; Wu, H.; Guo, S.; Zhang, J. *ACS Nano* **2012**, *6*, 6592−6599.

(19) Matsushima, T.; Adach, C. *Chem. Mater.* **2008**, *20*, 2881−2883.

(20) Woo, C. H.; Holcombe, T. W.; Unruh, D. A.; Sellinger, A.; Frechet, J. M. J. *Chem. Mater.* **2010**, *22*, 1673−1679.

(21) Kim, Y.; Cook, S.; Tuladhar, S. M.; Choulis, S. A.; Nelson, J.; Durrant, J. R.; Bradley, D. D. C.; Giles, M.; Mcculloch, I.; Ha, C.-S.; Ree, M. *Nat. Mater.* **2006**, *5*, 197−203.

(22) Samanta, S.; Das, S.; Layek, R. K.; Chatterjee, D. P.; Nandi, A. K. *Soft Matter* **2012**, *8*, 6066−6072.

(23) Puniredd, S. R.; Kiersnowski, A.; Battagliarin, G.; Zajaczkowski, W.; Wong, W. W. H.; Kirby, N.; Mullen, K.; Pisula, W. *J. Mater. Chem. C* **2013**, *1*, 2433−2440.

(24) Das, S.; Samanta, S.; Chatterjee, D. P.; Nandi, A. K. *J. Polym. Sci., Part A: Polym. Chem.* **2013**, *51*, 1417−1427.

(25) Scheblykin, I. G.; Yartsev, A.; Pullerits, T.; Gulbinas, V.; Sundstrom, V. *J. Phys. Chem. B* **2007**, *111*, 6303−6321.

(26) Meng, K.; Ding, Q.; Wang, S.; He, Y.; Li, Y.; Gong, Q. *J. Phys. Chem. B* **2010**, *114*, 2602−2606.

(27) Chang, Y.-T.; Hsu, S.-L.; Su, M.-H.; Wei, K.-H. *Adv. Funct. Mater.* **2007**, *17*, 3326−3331.

(28) Chen, H.-Y.; Hou, J.; Zhang, S.; Liang, Y.; Yang, G.; Yang, Y.; Yu, L.; Wu, Y.; Li, G. *Nat. Photonics* **2009**, *3*, 649−653.

(29) Park, S. H.; Roy, A.; Beaupre, S.; Cho, S.; Coates, N.; Moon, J. S.; Moses, D.; Leclerc, M.; Lee, K.; Heeger, A. J. *Nat. Photonics* **2009**, *3*, 297−303.

(30) Xie, Y.; Li, Y.; Xiao, L.; Qiao, Q.; Dhakal, R.; Zhang, Z.; Gong, Q.; Galipeau, D.; Yan, X. *J. Phys. Chem. C* **2010**, *114*, 14590−14600.

(31) Gupta, V.; Chaudhary, N.; Srivastava, R.; Sharma, D. G.; Bhardwaj, R.; Chand, S. *J. Am. Chem. Soc.* **2011**, *133*, 9960−9963.

(32) Das, S.; Chatterjee, D. P.; Samanta, S.; Nandi, A. K. *RSC Adv.* **2013**, *3*, 17540−17550.

(33) Fang, M.; Wang, K.; Lu, H.; Yang, Y.; Nutt, S. *J. Mater. Chem.* **2009**, *19*, 7098−7105.

(34) Routh, P.; Das, S.; Nandi, A. K. *RSC Adv.* **2012**, *2*, 11295−11305.

(35) Wang, Q.; Zheng, H.; Long, Y.; Zhang, L.; Gao, M.; Bai, W. *Carbon* **2011**, *49*, 3134−3140.

(36) Li, L. L.; Ji, J.; Fei, R.; Wang, C. Z.; Lu, Q.; Zhang, J. R.; Jiang, L. P.; Zhu, J. J. *Adv. Funct. Mater.* **2012**, *22*, 2971−2979.

(37) Pan, D.; Zhang, J.; Li, Z.; Wu, M. *Adv. Mater.* **2010**, *22*, 734−738.

(38) Radovic, L. R.; Bockrath, B. *J. Am. Chem. Soc.* **2005**, *127*, 5917.

(39) Lee, E.; Ryu, J.; Jang, J. *Chem. Commun.* **2013**, *49*, 9995−9997.

(40) Monguzzi, A.; Tubino, R.; Hoseinkhani, S.; Campione, M.; Meinardi, F. *Phys. Chem. Chem. Phys.* **2012**, *14*, 4322−4332.

(41) Ohta, T.; Bostwick, A.; Seyller, T.; Horn, K.; Rotenberg, E. *Science* **2006**, *313*, 951−954.

(42) Zhou, S. Y.; Gweon, G. H.; Fedorov, A. V.; First, P. N.; De Heer, W. A.; Lee, D. H.; Guinea, F.; Castro Neto, A. H.; Lanzara, A. *Nat. Mater.* **2007**, *6*, 770−775.

(43) Samanta, S.; Chatterjee, D. P.; Manna, S.; Mandal, A.; Garai, A.; Nandi, A. K. *Macromolecules* **2009**, *42*, 3112−3120.

(44) Chitara, B.; Krupanidhi, S. B.; Rao, C. N. R. *Appl. Phys. Lett.* **2011**, *99* (113114), 1−3.

(45) Chatterjee, S.; Patra, A. K.; Bhaumik, A.; Nandi, A. K. *Chem. Commun.* **2013**, *49*, 4646−4648.

(46) Chatterjee, S.; Shit, A.; Nandi, A. K. *J. Mater. Chem. A* **2013**, *1*, 12302−12309.

(47) Gunes, S.; Neugebauer, H.; Sariciftci, N. S. *Chem. Rev.* **2007**, *107*, 1324−1338.

(48) Li, W.; Roelofs, W. S. C.; Wienk, M. M.; Janssen, R. A. J. *J. Am. Chem. Soc.* **2012**, *134*, 13787−13795.

(49) Thompson, B. C.; Frechet, J. M. J. *Angew. Chem., Int. Ed.* **2008**, *47*, 58−77.

(50) Lu, S.-Y.; Lin, I.-H. *J. Phys. Chem B* **2003**, *107*, 6974−6978.

(51) Liu, Q.; Liu, Z.; Zhang, X.; Zhang, N.; Yang, L.; Yin, S.; Chen, Y. *Appl. Phys. Lett.* **2008**, *92*, 223−303.

(52) Li, F.; Kou, L.; Chen, W.; Wu, C.; Guo, T. *NPG Asia Mater.* **2013**, *5*, 1−4.